FOURIER TRANSFORMS, OPTION PRICING AND CONTROLS

MARK JOSHI AND CHAO YANG

ABSTRACT. We incorporate a simple and effective control-variate into Fourier inversion formulas for vanilla option prices. The control-variate used in this paper is the Black-Scholes formula whose volatility parameter is determined in a generic non-arbitrary fashion. We analyze contour dependence both in terms of value and speed of convergence. We use Gaussian quadrature rules to invert Fourier integrals, and numerical results suggest that performing the contour integration along the real axis leads to the best pricing performance.

1. INTRODUCTION

The Black–Scholes model whilst robust has many imperfections. One of these is that the volatilities implied by the market prices of vanilla options exhibit a smile- or skew-shaped graph against different strike levels. Over recent years, more complicated financial models have been introduced to address this empirical fact. For example, Heston (1993) developed a stochastic volatility model where the variance process is assumed to follow a square-root process, and Carr *et al* (1998) introduced the Variance-Gamma model where the log price follows a pure jump process with independent increments.

The advantage of implementing these more realistic models is that they partly solve the volatility smile issue. However, simple analytical formulas for vanilla option prices no longer exist and fast numerical methods are required to calculate the price. In this paper, we focus on using Fourier inversion methods to price vanilla options in complicated financial models for calibration purposes since analytical forms of the characteristic functions of the underlying process have much simpler functional forms than the density functions in these aforementioned models.

Stein and Stein (1991) and Heston (1993) were among the first to introduce Fourier transform (in the log-forward space) methods in finance. In particular, Heston (1993) derived a semi-closed-form solution for European call and put options in his stochastic volatility model. Carr and Madan (1999) developed a pricing approach based on the Fourier-Laplace transform in the log-strike space, and they showed how to calculate the Fourier integral using fast Fourier transform (FFT). Lewis (2001) derived general pricing formulas using the Fourier-Laplace transform in log-forward space and analyzed the behaviour of these integrals using complex analysis and considered contour shifting. Borovkov and Novikov (2002) independently introduced a similar approach. Lee (2004) carried out a detailed error analysis of the Carr-Madan approach. Dufresne *et al* (2009) studied how to apply Fourier inversion methods to insurance premium pricing problems.

However, the general pricing formulas derived in Carr and Madan (1999) and Lewis (2001) have an issue in terms of practical implementation. The Fourier integrands are found to have poles in the complex plane so the value of the Fourier integral varies with the choice of contour. Carr and Madan (1999) introduced a time-value approach which allowed the use of the regular Fourier transform rather than generalized versions, but its usefulness was questioned in a detailed study carried out in Matsuda (2004).

A control-variate approach has been suggested in Andersen and Andreasen (2002), Itkin (2005) and Andersen and Piterbarg (2010). The control variate chosen is the Black–Scholes price of an

1

option with the same contract parameters and interest rates. However, one has still has to choose a volatility and this has typically been done in *ad hoc* fashion.

In this paper, we analyze the integrals that arise when using a control variate. Our starting point is the representation of Carr and Madan (1999), however, our philosophy and overall approach is closer to that of Lewis (2001). We see that in contrast to the uncontrolled case, the theoretical value of the integral does not depend on the choice of horizontal contour. We suggest a choice of volatility that makes the controlled intregrand zero at the pure imaginary point and perform numerical experiments to test its efficacy. We also compare choices of contours. In particular, we look at using the real axis versus the commonly chosen contour of imaginary part $1/2$, and we see that the former is more effective.

Kilin (2011) showed that if we cache the values of the characteristic functions then the calibration with direct integration methods is at least seven times faster than that with the FFT methods. Therefore, we use Gaussian quadrature rules to approximate Fourier integrals in our new pricing formulas. Numerical results show that our new approach is highly accurate and produces robust results across different testing cases.

The paper is organized as follows. We give a brief review on the Carr-Madan approach in section 2. In section 3, we investigate different methodologies that incorporates control-variates for calculating Fourier integrals. Numerical results are shown in section 4. We conclude in section 5. Formulas for the first derivatives of characteristic functions are given in the appendix.

We are grateful to Alan Lewis for his comments on a previous version of this paper.

2. Review of the Carr-Madan Approach

In contrast to Carr and Madan (1999), we will be working with the forward price, which is a martingale under the forward pricing measure. We denote by $F_T(t)$ the time-t forward price of some stocks with spot price S and maturity T. From simple no-arbitrage arguments, F_T is given by

$$F_T(t) = S(t)e^{r(T-t)}, \quad 0 \leq t \leq T, \tag{2.1}$$

where r is the risk-free rate. We model the log-forward prices with a càdlàg stochastic process X (e.g., a continuous diffusion process or a Lévy process):

$$F_T(t) = e^{X(t)}. \tag{2.2}$$

In many financial applications, the characteristic function of the terminal log-forward price

$$\hat{\psi}_T(\xi) = \mathbb{E}\left(e^{i\xi \log F_T(T)}\right) = \mathbb{E}\left(e^{i\xi X(T)}\right) \tag{2.3}$$

has a closed-form solution. Examples include the stochastic volatility model proposed by Heston (1993) and the Variance-Gamma model studied in Carr *et al* (1998). Since we are working in the forward measure, we have that the expectation of the terminal forward price is equal to its current value; that is

$$\psi_T(-i) = \mathbb{E}\left(S_T\right) = F_T(0).$$

2.1. **Fourier transform in the log-strike space.** We briefly review the Carr-Madan (1999) approach. Assuming that the density function of $X(T)$ under the forward measure, ψ_T, exists, we can write the price of a European call with maturity T and strike K as the following integral

$$C(l, T) = e^{-rT} \int_{\mathbb{R}} \left(e^x - e^l\right)^+ \psi_T(x) \mathrm{d}x, \tag{2.4}$$

where $l = \log K$. In situations where the functional form of the characteristic function is simpler than the original density function, Fourier transform methods can be efficiently adopted to compute European-type options such as (2.4). In this paper, we take the Fourier transform of C in the log-strike space as in Carr and Madan (1999). Note that we could also take Fourier transforms in the log-forward space.

In log-strike space, the call price C is not integrable as $\lim_{l \to -\infty} C(l, T) = S(0)$. Hence, Carr and Madan (1999) considered a modified call price $e^{-\eta l} C(l, T)$, $\eta < 0$, such that the Fourier transform exists. Their approach is equivalent to taking the Fourier-Laplace transform[1] of $C(l, T)$ in log-strike space: let $z = \xi + i\eta$ with $\eta < 0$ and provided that $\mathbb{E}(S(T)^{1-\eta}) < \infty$, then we have

$$\hat{C}_\eta(z) = \int_{\mathbb{R}} e^{izl} C(l, T) \mathrm{d}l = \frac{e^{-rT} \hat{\psi}_T(z - i)}{z(i - z)}. \tag{2.5}$$

The price of the European call option is recovered from the inversion of (2.5):

$$C(l, T) = \frac{1}{2\pi} \int_{\Gamma_\eta} e^{-izl} \hat{C}_\eta(z) \mathrm{d}z = \frac{K^\eta}{\pi} \int_0^\infty \mathrm{Re}\Big(e^{-i\xi l} \hat{C}_\eta(\xi + i\eta) \Big) \mathrm{d}\xi, \tag{2.6}$$

where $\Gamma_\eta = \{z \in \mathbb{C} : z = \xi + i\eta, \xi \in \mathbb{R}\}$ is the integration contour. The integral in (2.6) can be evaluated numerically by direct integration or FFT.

2.2. **The time-value approach.** As pointed out by Carr and Madan (1999), there are numerical issues when we work with options with very short maturities. Hence, they suggested working with time-values of out-of-the-money options; i.e., put options for strikes below spot and call options for strikes above spot. They defined an integrable function $z_T(l)$ by

$$z_T(l) = e^{-rT} \int_{\mathbb{R}} \left(\left(e^l - e^x \right)^+ \mathbb{I}_{\{l < \log S(0)\}} + \left(e^x - e^l \right)^+ \mathbb{I}_{\{l > \log S(0)\}} \right) \psi_T(x) \mathrm{d}x. \tag{2.7}$$

The Fourier transform of z_T is given by

$$\hat{z}_T(\xi) = \int_{\mathbb{R}} e^{i\xi l} z_T(l) \mathrm{d}l = e^{-rT} \left(\frac{1}{1 + i\xi} - \frac{e^{rT}}{i\xi} - \frac{\hat{\psi}_T(\xi - i)}{\xi^2 - i\xi} \right). \tag{2.8}$$

Carr and Madan (1999) studied the shape of $\hat{z}_T$ and found out that $\hat{z}_T$ approximates a Dirac delta function for l close to $\log S(0)$, they therefore suggest working with the Fourier transform of $\sinh(\alpha l) z_T(l)$.

However, as pointed out in McCulloch (2003), we can also make the transition from put to call based on forward price. We define a function $D_T(l)$ by

$$D_T(l) = e^{-rT} \int_{\mathbb{R}} \left(\left(e^l - e^x \right)^+ \mathbb{I}_{\{l < \log F_T(0)\}} + \left(e^x - e^l \right)^+ \mathbb{I}_{\{l > \log F_T(0)\}} \right) \psi_T(x) \mathrm{d}x. \tag{2.9}$$

Let $z = \xi + i\eta$, the Fourier-Laplace transform of (2.9) is given by

$$\hat{D}_T(z) = \int_{\mathbb{R}} e^{izl} D_T(l) \mathrm{d}l = \frac{e^{-rT}}{z^2 - iz} \Big(\big(\mathbb{E}(S(T))\big)^{iz+1} - \hat{\psi}_T(z - i) \Big). \tag{2.10}$$

Note that $\hat{D}_T$ decays at a quadratic rate, which is faster than that of $\hat{z}_T$ in (2.8). Now, we have $\hat{\psi}_T(-i) = \mathbb{E}(S(T))$ and $\hat{\psi}_T(0) = 1$ so that the poles at $z = 0$ and $z = i$ are removable poles. The function D_T can be recovered from inverting the transform $\hat{D}_T$

$$D_T(l) = \frac{1}{2\pi} \int_{\Gamma_\eta} e^{-izl} \hat{D}_T(z) \mathrm{d}z. \tag{2.11}$$

Matsuda (2004) performed an in-depth analysis of the Carr-Madan time-value approach. In particular, Matsuda applied the method to the classical Black-Scholes model to price European call or put options, and found out the time-value approach is possibly inferior to directly evaluating (2.6). However, we will see in section 4, the time-value approach will be able to compute extremely accurate prices in almost negligible amount of time after we have incorporated effective control-variates into (2.10).

---

[1]This transform is sometimes called the generalized Fourier transform.

3. Fourier Inversion Methods with Control-Variates

In stochastic volatility type models, Andersen and Andreasen (2002) showed how to incorporate Black's formula as a control-variate to price European swaptions in a LIBOR market model. Andersen and Piterbarg (2010) derived similar Fourier integrals with the Black-Scholes formula control-variate to price European call options in an extended Black-Scholes model with stochastic volatility. In these studies, the unknown volatility parameter in the Black-Scholes formula is arbitrarily set equal to either a simple function of the initial volatility or the at-the-money implied volatility, which can be approximated by asymptotic expansion techniques (see Lewis (2000)).

Itkin (2005) used the Black-Scholes formula as a control-variate to price European call options in the Variance-Gamma model. The volatility parameter is set equal to one of the Variance-Gamma model parameters.

Due to the existence of a simple analytical pricing formula, we also use the Black-Scholes formula as our first control-variate. Specifically, we give a simple algorithm on how to analytically compute the unknown volatility parameter. We then introduce our second control-variate, which is a simple complex polynomial multiplied by exponential functions, to further improve the convergence of the controlled Fourier integrals.

3.1. General pricing formula with the Black-Scholes formula control-variate.

In the classical Black-Scholes (1973) model, X in (2.2) is modelled by a Brownian motion with drift:

$$X(T) = \log F_T(0) - \frac{\sigma^2 T}{2} + \sigma \widetilde{W}_T,$$

where $\widetilde{W}$ is a Brownian motion under the forward pricing measure. The characteristic function of X is given by

$$\hat{\psi}_T^{bs}(\xi) = F_T(0)^{\mathrm{i}\xi} \exp\left(\frac{-\sigma^2 T}{2}\left(\mathrm{i}\xi + \xi^2\right)\right). \tag{3.1}$$

Note that if we work with the Black-Scholes model, the left-hand-side of (2.11) is given by the Black-Scholes pricing formula. Hence, adding the pricing formula and subtracting its Fourier integral in (2.11) gives the following general pricing formula in a more complicated financial model:

$$D_T(l) = \frac{1}{2\pi} \int_{\Gamma_\eta} e^{-\mathrm{i}zl} \hat{\phi}(z) \mathrm{d}z + \mathrm{BS}\big(S(0), K, r, T; \sigma\big), \tag{3.2}$$

where $\mathrm{BS}\big(S(0), K, r, T; \sigma\big)$ returns the Black-Scholes price (put if $K < F_T(0)$ and call otherwise) and

$$\hat{\phi}(z) = \frac{e^{-rT}}{z(z-\mathrm{i})}\left(\hat{\psi}_T^{bs}(z-\mathrm{i}) - \hat{\psi}_T(z-\mathrm{i})\right). \tag{3.3}$$

In fact, although we have derived this formula only to hold for out-of-the-money options, it is immediate from put-call parity that it will hold also for in-the-money options simply by using the appropriate version of the Black–Scholes formula.

We emphasize here that the integrand $\hat{\phi}$ does not have poles, we summarize its properties:

Theorem 3.1. *Let U be an open subset of $\mathbb{C}$. If $\hat{\psi}_T$ is analytic in U then so is $\hat{\phi}$. In addition, if*

$$|\hat{\psi}_T(\xi + \mathrm{i}\eta)| \le C_\eta (1 + |\xi|)^{-N}$$

for some C_η, N and fixed $\eta \in \mathbb{R}$, then there exists $\tilde{C}_\eta$ such that

$$|\hat{\phi}(\xi + \mathrm{i}\eta)| \le \tilde{C}_\eta (1 + |\xi|)^{-N-2}.$$

Proof. The Black-Scholes characteristic function $\hat{\psi}_T^{bs}$ is an entire function in $\mathbb{C}$. The poles of $\hat{\phi}$ at 0 and i are removable poles since $\hat{\psi}_T^{bs}(z) = \hat{\psi}_T(z)$ at $z = 0$ and $z = \mathrm{i}$. Hence, $\hat{\phi}$ is analytic in U given that $\hat{\psi}_T^{bs} - \hat{\psi}_T$ is analytic in U. To prove the decay, observe that the Black–Scholes characteristic

function is exponentially decaying so the results follows from the fact that the reciprocal of a quadratic decays to second order. $\quad\square$

The fact that $\hat{\phi}$ decays two orders faster than the characteristic function is one reason for the power of the control-variate technique, contrast this with (2.10) where we only have second order decay, or (2.8) where the decay is first order.

3.2. **Invariance of contour integration.** Lewis (2001) derived general option pricing formulas in exponential Lévy models using residue calculus results. Depending on the chosen integration contour horizontal to the real axis, his pricing formulas have different representations due to the existence of poles in the complex plane. However, since the integrand $\hat{\phi}$ has no poles, this is not an issue with our approach.

Definition 3.1. *The strip of regularity of a characteristic function $\hat{\psi}_T$ is the largest set in $\mathbb{C}$ of the form $\mathcal{S}_X = \{z = \xi + i\eta : \xi \in \mathbb{R} \text{ and } \alpha < \eta < \beta\}$, for some $\alpha < 0, \beta > 0 \in \mathbb{R}$, such that $\hat{\psi}_T$ both exists and is analytic in $\mathcal{S}_X$.*

Theorem 3.2. *The value of the following contour integral*

$$\int_{\Gamma_\eta} e^{-izl}\hat{\phi}(z)\mathrm{d}z,$$

where $\Gamma_\eta = \{z = \xi + i\eta : \xi \in \mathbb{R}\}$ and $\hat{\phi}$ is as specified in (3.3), is independent of η provided that $\{z - i : z \in \Gamma_\eta\} \subseteq \mathcal{S}_X$.

Proof. Let the integration contour as in the statement of the theorem be Γ_S. We integrate $e^{-izl}\hat{\phi}(z)$ round the rectangle with vertices at $-R$, R, $R + iS$, $-R + iS$ (shown in figure 1). It is clear that the rectangular path is a subset of $\mathcal{S}_X$, and by Cauchy's theorem (see Priestley (2003)):

$$\int_{-R}^{R} e^{-i\xi l}\hat{\phi}(\xi)\mathrm{d}\xi + \int_{0}^{S} e^{-i(R+i\eta)l}\hat{\phi}(R + i\eta)\mathrm{d}\eta$$
$$+ \int_{R}^{-R} e^{-i(\xi+iS)l}\hat{\phi}(\xi + iS)\mathrm{d}\xi + \int_{S}^{0} e^{-i(-R+i\eta)l}\hat{\phi}(-R + i\eta)\mathrm{d}\eta = 0.$$

Now, notice that

$$\left|\hat{\psi}_T(R + i\eta)\right| \leq \int_{\mathbb{R}} \left|e^{i(R+i\eta)x}\right|\psi_T(x)\mathrm{d}x = \hat{\psi}_T(i\eta).$$

The function $\hat{\psi}_T(i\eta)$ is continuous for $\eta \in [0, S]$ so $\hat{\psi}_T(i\eta)$ is bounded for $\eta \in [0, S]$, independently of R. Consequently, $\left|\hat{\psi}_T(R + i\eta)\right|$ is bounded for all $\eta \in [0, S]$. Since both of $|\hat{\psi}_T^{bs}|$ and $|\hat{\psi}_T|$ are bounded on the vertical lines, we have

$$\left|\int_{0}^{S} e^{-i(R+i\eta)l}\hat{\phi}(R + i\eta)\mathrm{d}\eta\right| \leq C\frac{S}{R^2}$$

for some C. This clearly goes to zero as R goes to infinity. Similarly, for the left-side of the contour. We conclude

$$\int_{\mathbb{R}} e^{-i\xi l}\hat{\phi}(\xi)\mathrm{d}\xi = \lim_{R\to\infty}\int_{-R}^{R} e^{-i\xi l}\hat{\phi}(\xi)\mathrm{d}\xi = \lim_{R\to\infty}\int_{-R}^{R} e^{-i(\xi+iS)l}\hat{\phi}(\xi + iS)\mathrm{d}\xi = \int_{\Gamma_S} e^{-izl}\hat{\phi}(z)\mathrm{d}z. \quad\square$$
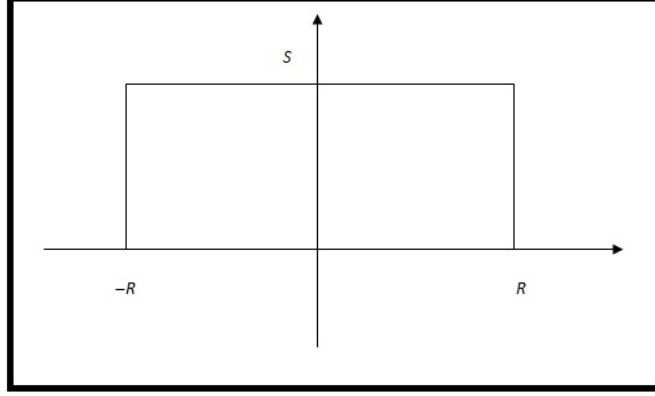
FIGURE 1. Integration contour for $e^{-izl}\hat{\phi}(z)$. The direction of the rectangular path is anti-clockwise.

3.3. Computing the volatility parameter.

Depending on the imaginary part of z in (3.3), we have three cases:

1. If $\text{Im}(z) = \eta \neq 0$ or 1 (i.e., we carry out integration on a line parallel to $\mathbb{R}$), then we choose σ such that the two characteristic functions agree with each other at $i(\eta - 1)$ (i.e., $\hat{\phi}(i\eta) = 0$):

$$\sigma^2 = \frac{2\log\left(\hat{\psi}_T(i(\eta - 1))\right)}{\eta(\eta - 1)T} = \frac{2}{\eta(\eta - 1)T}\log\left(\mathbb{E}\left(F_T(T)^{(1-\eta)}\right)\right). \tag{3.4}$$

2. If $\text{Im}(z) = \eta = 0$, then the two characteristic functions agree with each other at $-i$. We therefore have to choose σ such that $\left(\hat{\psi}_T\right)'$ agrees with $\left(\hat{\psi}_T^{bs}\right)'$ at $-i$:

$$\sigma^2 = \frac{2}{T}\text{Im}\left(\left(\hat{\psi}_T\right)'(-i)\right), \tag{3.5}$$

and we have matched $\mathbb{E}\left(F_T(T)\log F_T(T)\right)$ in both models.

3. If $\text{Im}(z) = \eta = 1$, the two characteristic functions agree with each other at the origin, and we again choose σ such that $\left(\hat{\psi}_T\right)'$ agrees with $\left(\hat{\psi}_T^{bs}\right)'$ there

$$\sigma^2 = -\frac{2}{T}\text{Im}\left(\left(\hat{\psi}_T\right)'(0)\right), \tag{3.6}$$

and we have matched $\mathbb{E}\left(\log F_T(T)\right)$ in both models.

3.4. Choice of the contour and two generic pricing formulae.

The choice of η in (3.2) is arbitrary; we focus on two special cases in this paper:

1. If we set $\eta = 1/2$ then (3.3) will be Hermitian [2] so that we can rewrite (3.2) as

$$D_T(l) = \frac{\sqrt{K}}{\pi}\int_0^\infty \text{Re}\left(e^{-i\xi l}\hat{\phi}_{0.5}(\xi)\right)d\xi + \text{BS}\left(S(0), K, r, T; \sigma\right), \tag{3.7}$$

where

$$\hat{\phi}_{0.5}(\xi) = \frac{e^{-rT}}{\xi^2 + 1/4}\left(\hat{\psi}_T^{bs}(\xi - i/2) - \hat{\psi}_T(\xi - i/2)\right). \tag{3.8}$$

Note that $i/2$ is the furthest point from the singularities of $(z(z - i))^{-1}$ within $0 < \text{Im } z < 1$. In addition, all the terms in (3.8) are real except $\hat{\psi}_T$, this means that oscillations will only arise if they were already present in the characteristic function. The reality of terms also reduces the amount of complex arithmetic required, and this leads to a fast numerical implementation.

---

[2] A function f is Hermitian if $f(-\xi) = \overline{f(\xi)}$. Therefore, $\int_{\mathbb{R}} f(\xi)d\xi = 2\int_0^\infty \text{Re}(f(\xi))d\xi$.

2. If we set $\eta = 0$ then (3.3) will also be Hermitian. We then rewrite (3.2) as

$$D_T(l) = \frac{1}{\pi} \int_0^\infty \mathrm{Re}\Big(e^{-\mathrm{i}\xi l}\hat{\phi}_0(\xi)\Big)\mathrm{d}\xi + \mathrm{BS}\big(S(0), K, r, T; \sigma\big), \qquad (3.9)$$

where

$$\hat{\phi}_0(\xi) = \frac{e^{-rT}}{\xi(\xi - \mathrm{i})}\Big(\hat{\psi}_T^{bs}(\xi - \mathrm{i}) - \hat{\psi}_T(\xi - \mathrm{i})\Big). \qquad (3.10)$$

In contrast to (3.8), the denominator term in (3.10) is complex-valued so that it is expected that numerical implementation of (3.9) will be slower than (3.7). However, as we will see from the numerical tests in section that the improvement in the accuracy level outweighs the increase in the computational time.

4. Numerical Results

In this section, we perform a variety of numerical tests to investigate the effectiveness of the control-variates. Note that we work with unit forward prices since European call and put options are homogeneous of order 1 in $(F_T(0), K)$. We consider two financial models where the characteristic function of the terminal log-forward price has a closed-form solution.

4.1. **Homogeneity of European call and put options.** For log-type models such as (2.2), the price of European call and put options is homogeneous of order 1 in $(S(0), K)$: for any $\lambda > 0$,

$$C(\lambda F_T(0), \lambda K) = e^{-rT} \int_{\mathbb{R}} \big(\lambda F_T(0)e^x - \lambda K\big)^+ \psi_T(x)\mathrm{d}x = \lambda C(F_T(0), K). \qquad (4.1)$$

Thus, we can work with a unit current forward price and the corresponding strike (i.e., $K/F_T(0)$). The put case can be derived similarly.

We suggest this approach in pricing vanilla options using Fourier inversion methods. The main reason is that it takes less time to compute characteristic functions since we do not need to calculate $F_T(0)^{\mathrm{i}\xi}$ in the Black-Scholes characteristic function (3.1) and other characteristic functions shown below.

4.2. **Popular financial models.** The Heston stochastic volatility model specifies the terminal log-forward price as a continuous diffusion process, and is well-known to be able to capture the volatility smile observed in equity and foreign exchange derivative markets. The Variance-Gamma model specifies the underlying log-forward price as a pure jump process, and is able to capture the non-negligible probability of sudden large changes in forward prices within a short period of time.

4.2.1. *The Heston stochastic volatility model.* The dynamics of the diffusion process X in (2.2) under the risk-neutral measure is given by

$$X(T) = \log F_T(0) - \frac{1}{2} \int_0^T v(t)\mathrm{d}t + \int_0^T \sqrt{v(t)}\mathrm{d}\widetilde{W}_F(t), \qquad (4.2)$$

where $\widetilde{W}_F$ is a Brownian motion. The dynamics of the variance process v, under the pricing measure, is modelled by the following square root process

$$\mathrm{d}v(t) = \kappa\big(\theta - v(t)\big)\mathrm{d}t + \sigma\sqrt{v(t)}\mathrm{d}\widetilde{W}_v(t), \qquad (4.3)$$

where κ is the mean-reversion speed, θ is the long-term mean, σ is the volatility of volatility, and $\widetilde{W}_v$ is a Brownian motion correlated to $\widetilde{W}_F$ with instantaneous correlation ρ.

There are two forms of the characteristic function of $X(T)$ in the literature: the original one derived in Heston (1993) and the one given in Gatheral (2005). Albrecher *et al* (2006) showed that the original functional form is subject to numerical instabilities while the stability of the second

form is guaranteed under the full dimensional and unrestricted parameter space. We adopt the second form of the characteristic function:

$$\hat{\psi}_T^h(\xi) = F_T(0)^{i\xi} \exp\left(\frac{\kappa\theta}{\sigma^2}\left(A_-(\xi)T - 2\log\left(\frac{1 - g(\xi)e^{-d(\xi)T}}{1 - g(\xi)}\right)\right) + \frac{v(0)}{\sigma^2}\frac{A_-(\xi)\left(1 - e^{-d(\xi)T}\right)}{1 - g(\xi)e^{-d(\xi)T}}\right), \quad (4.4)$$

where

$$d(\xi) = \sqrt{\left(i\rho\sigma\xi - \kappa\right)^2 + \sigma^2\left(i\xi + \xi^2\right)}, \quad A_\pm(\xi) = \kappa - i\rho\sigma\xi \pm d(\xi), \quad g(\xi) = \frac{A_-(\xi)}{A_+(\xi)}. \quad (4.5)$$

4.2.2. *The Variance-Gamma model.* The evolution of the process X in (2.2) is modelled by a time-changed Brownian motion

$$X(T) = \log F_T(0) + \omega T + \left(\theta\Gamma(T) + \sigma\widetilde{W}\left(\Gamma(T)\right)\right), \quad (4.6)$$

where $\Gamma(T)$ is a Gamma process with parameter ν, $\omega = \nu^{-1}\log(1 - \theta\nu - \sigma^2\nu/2)$ and $\widetilde{W}$ is a Brownian motion under the risk-neutral measure.

Carr *et al* (1998) showed that the characteristic function of $X(T)$ is

$$\hat{\psi}_T^{vg}(\xi) = F_T(0)^{i\xi} \exp\left(i\xi\omega T - \frac{T}{\nu}\log\left(1 - i\theta\nu\xi + \frac{1}{2}\sigma^2\nu\xi^2\right)\right). \quad (4.7)$$

Lewis (2001) stated that the strip of regularity of $\hat{\psi}_T^{vg}$ is the set $\{z = \xi + i\eta : \xi \in \mathbb{R} \text{ and } \alpha_- < \eta < \alpha_+\}$ where

$$\alpha_\pm = \frac{\theta}{\sigma^2} \pm \sqrt{\frac{2}{\nu\sigma^2} + \frac{\theta^2}{\sigma^4}}. \quad (4.8)$$

In the Variance-Gamma testing cases presented in table 4.1, our choice of $\eta = 0.5$ satisfies (4.8).

4.2.3. *Discontinuity issues in characteristic function evaluations.* The complex logarithm and power functions in (4.4) and (4.7) are multi-valued functions. In some cases, if we restrict the logarithm naively to its principal branch then the characteristic function will become discontinuous, leading to erroneous option prices.

Lord and Kahl (2010) proved that, in both of these two models even though we compute the complex logarithm and power using their principal branch, there will not be discontinuity problems in evaluating the characteristic functions (4.4) and (4.7) without any restrictions on parameters. Hence, it is straightforward to code up programs to compute the Heston and Variance-Gamma characteristic functions in standard languages such as C++.

4.3. **Model parameter sets.** The test cases are given in table 4.1:

- The Heston parameters are taken from Andersen (2007), which states that case I is a representative of the market for long-dated FX options, case II is that for long-dated interest-rate options, and case III is that for equity options.
- The Variance-Gamma parameters are taken from Carr and Madan (1999).

According to the homogeneity property of vanilla call and put options, we work with a unit forward price in all cases. For simplicity, we assume zero interest-rate (i.e., $\lambda = 1$).

4.4. **Testing pricing algorithms.** We will investigate the following five different pricing algorithms for computing vanilla options:

- The original Carr-Madan method (2.6) with $\eta = 0.5$ (CM).
- The control-variate algorithm (3.7) with the Black-Scholes volatility parameter set to the initial volatility in the Heston model or the parameter σ in the Variance-Gamma model (AP1).
- The control-variate algorithm (3.7) with the Black-Scholes volatility parameter given by (3.4) (CV1).

	Heston stochastic volatility model						Variance-Gamma model			
Case	κ	θ	σ	ρ	T	$v(0)$	ν	θ	σ	T
I	0.5	0.04	1.0	-0.9	10	0.04	2.00	-0.10	0.25	1.00
II	0.3	0.04	0.9	-0.5	15	0.04	0.16	-0.33	0.12	0.25
III	1.0	0.09	1.0	-0.3	5	0.09				

TABLE 4.1. Test cases for the Heston stochastic volatility model and the Variance-Gamma model, in all cases $S(0) = 1$ and $r = 0$.

- The control-variate algorithm (3.9) with the Black-Scholes volatility parameter set to the initial volatility in the Heston model or the parameter σ in the Variance-Gamma model (AP2).
- The control-variate algorithm (3.9) with the Black-Scholes volatility parameter given by (3.5) (CV2).

We first study the convergence behaviour of the five complex-valued integrands, we then perform numerical analysis on the accuracy level of the five pricing algorithms.

4.4.1. *Integrand convergence.* The plot of the real part of the five complex-valued integrands are shown in figures 2 to 6. For the Heston stochastic volatility model, we observe that:

- If the Black-Scholes volatility is computed by matching the value or the first derivative of the two characteristic functions at $-\mathfrak{i}$, then we see that performing the contour integration on the real axis (CV2) results in faster convergence of the integrand over all three cases.
- If the Black-Scholes volatility is set to the initial volatility, then performing the contour integration on the real axis does not result in a faster convergence of the integrand.
- Performing the contour integration on the real axis and computing the Black-Scholes volatility using (3.5) results in the fastest convergence rate in all three cases (CM gives the worst outcome).

For the Variance-Gamma model, we have similar observations as in the Heston model; i.e., performing the integration along the real axis and computing the Black-Scholes volatility via matching the first derivatives of the two characteristic functions at $-\mathfrak{i}$ results in the fastest convergence rate. However, it is clear from figures 5 and 6 that the convergence of integrands is slower in the Variance-Gamma model; in particular, the shorter the maturity, the slower the convergence rate.

Hence, in the following numerical tests, we will then only focus on the following three pricing algorithms: CV2, AP1 and AP2.

4.4.2. *Pricing performance.* For each of the testing cases in table 4.1, we compute the true price of a vanilla option according to different levels of the strike price via approximating (3.9) with a 150-point Gauss-Laguerre quadrature rule. We then compute the price of the option using the aforementioned three pricing algorithms with different number of integration points. We always use whichever of the call and the put that is out of the money. The pricing errors of the CV2 algorithm and the ratios of the pricing errors of the AP1 and AP2 algorithms to those of the CV2 algorithm are shown in tables 4.2 to 4.11. All tests are carried out using single-threaded C++ code on a notebook computer[3].

For the numerical tests carried out in the Heston stochastic volatility model, we observe that:

1. In test case I:
    - the CV2 pricing error converges rapidly; in particular, we see that all pricing errors are less than one bp with the number of integration points equal to 10;
    - we have an increased level of accuracy if we perform integration along the real axis;
    - it is not clear whether computing the Black-Scholes volatility using our new algorithm (3.5) results in any benefits.
2. In test case II:

---

[3]Intel Core i5 2.40GHz CPU and 4GB RAM.

Heston	case I	number of integration points										
strike	true price	5	6	7	8	9	10	11	12	13	14	15
0.80	772	-8.48	-5.09	2.68	1.56	-1.03	**-0.48**	0.45	0.16	-0.19	-0.04	0.08
0.85	883	3.33	-5.11	-2.07	1.24	0.93	**-0.25**	-0.37	0.04	0.15	0.01	-0.06
0.90	1007	9.41	0.84	-2.43	-1.22	0.30	**0.54**	0.12	-0.14	-0.10	0.01	0.04
0.95	1148	5.98	4.62	0.92	-0.83	-0.77	**-0.18**	0.16	0.16	0.05	-0.03	-0.04
1.00	1308	-2.87	2.30	2.39	1.08	0.09	**-0.27**	-0.23	-0.09	0.01	0.04	0.03
1.05	995	-9.35	-2.94	0.01	0.84	0.73	**0.39**	0.13	-0.01	-0.05	-0.05	-0.02
1.10	713	-7.75	-4.90	-2.51	-1.02	-0.26	**0.05**	0.14	0.12	0.08	0.04	0.02
1.15	475	1.13	-0.93	-1.20	-0.96	-0.66	**-0.41**	-0.23	-0.12	-0.06	-0.03	-0.01
1.20	290	9.39	4.46	2.17	1.07	0.52	**0.25**	0.11	0.04	0.01	0.00	0.00

TABLE 4.2. The pricing errors (in basis points) from the CV2 algorithm. The true prices are computed from approximating (3.9) with a 150-point Gauss-Laguerre quadrature rule. The Heston stochastic volatility model parameters are case I in table 4.1.

- the CV2 pricing error converges extremely fast; in particular, we see that all pricing errors are less than one bp with the number of integration points equal to 6;
- we have a substantially increased level of accuracy if we perform integration along the real axis;
- we have a marginally increased level of accuracy if we compute the Black-Scholes volatility using our new algorithm (3.5).

3. In test case III:
- the CV2 pricing error converges extremely fast; in particular, we see that all pricing errors are less than one bp with the number of integration points equal to 6;
- we have a substantially increased level of accuracy if we perform integration along the real axis;
- we have a substantially increased level of accuracy if we compute the Black-Scholes volatility using our new algorithm (3.5).

For the numerical tests carried out in the Variance-Gamma model, we have similar observations:

1. In test case I:
- the CV2 pricing error converges extremely fast; in particular, we see that all pricing errors are less than one bp with the number of integration points equal to 7;
- it is not clear whether performing the contour integration along the real axis or computing the Black-Scholes volatility using our new algorithm (3.5) results in any benefits.

2. In test case II:
- the CV2 pricing error converges relatively slowly, which corresponds to the observation of figure 6;
- we have an increased level of accuracy if we perform the integration along the real axis or compute the Black-Scholes volatility using our new algorithm (3.5).

We present the summary of these numerical tests in table 4.12. In all of the testing cases, performing the integration along the real axis or computing the volatility parameter of the Black-Scholes pricing formula control leads to either an (substantial) improvement in the level of accuracy or gives very similar pricing results. Therefore, we can conclude that the pricing algorithm (3.9) with the Black-Scholes volatility parameter given by (3.5) seems to be the most efficient approach for computing vanilla option price within complicated financial models.
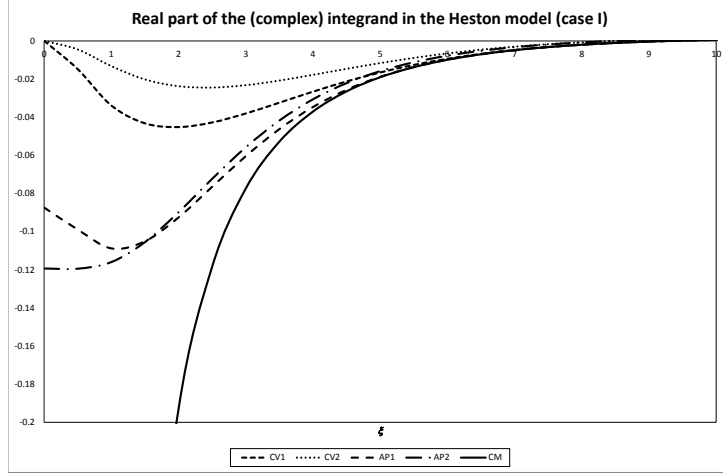
FIGURE 2. The solid line represents the real part of (2.5) with $\eta = 0.5$. The square dot line represents the real part of (3.8) with the Black-Scholes volatility given by (3.4). The dash line represents the real part of the same integrand with the Black-Scholes volatility equal to 0.2. The round dot line represents the real part of (3.10) with the Black-Scholes volatility given by (3.5). The dash dot line represents the real part of the same integrand with the Black-Scholes volatility equal to 0.2. The Heston stochastic volatility model parameters are case I in table 4.1.

5. Conclusion

we have successfully analyzed and improved the Black–Scholes control variate approach to inverting Fourier transforms of vanilla option prices. The first part to our approach is to compute the Black-Scholes volatility via matching the first derivatives of the Black-Scholes characteristic function and the characteristic function of the forward price process in the more complicated model. This methodology has the virtue of being model independent.

The second part to our approach is to perform the contour integration along the real axis whereas it was previously very common to perform the integration along the contour where the imaginary part of the complex number is equal to 0.5.

We have illustrated our methods for the Heston stochastic volatility model and the Variance-Gamma model, and found out that the additional computational complexity of this algorithm is minimal while the enhancement in accuracy level is significant. The high levels of accuracy is expected to improve the efficiency of real-time calibration to a large number of options for a wide range of financial models.

Appendix A. First Derivatives of Characteristic Functions

In this section, we give simple formulas to evaluate first and second derivatives of the characteristic function in the two models discussed in section 4.2. For simplicity and due to the homogeneity of call option pay-offs, we set the current forward price to 1.

A.1. **The Heston model.** The characteristic function of the log-forward price in the Heston model is given by (4.4). To simplify derivative computations, we introduce the following intermediate

FIGURE 3. The solid line represents the real part of (2.5) with $\eta = 0.5$. The square dot line represents the real part of (3.8) with the Black-Scholes volatility given by (3.4). The dash line represents the real part of the same integrand with the Black-Scholes volatility equal to 0.2. The round dot line represents the real part of (3.10) with the Black-Scholes volatility given by (3.5). The dash dot line represents the real part of the same integrand with the Black-Scholes volatility equal to 0.2. The Heston stochastic volatility model parameters are case II in table 4.1.

functions:

$$B(\xi) = \frac{b_1(\xi)}{b_2(\xi)}, \quad \text{with} \quad b_1(\xi) = 1 - g(\xi)e^{-d(\xi)T}, \quad b_2(\xi) = 1 - g(\xi), \tag{A.1}$$

$$C(\xi) = \frac{c_1(\xi)}{b_1(\xi)}, \quad \text{with} \quad c_1(\xi) = 1 - e^{-d(\xi)T}, \tag{A.2}$$

where d and g are given in (4.5). Thus, we can rewrite (4.4) as

$$\hat{\psi}_T^h(\xi) = \exp\left(\frac{\kappa\theta}{\sigma^2}\Big(A_-(\xi)T - 2\log B(\xi)\Big) + \frac{v(0)}{\sigma^2}A_-(\xi)C(\xi)\right). \tag{A.3}$$

Using simple chain rules, the first derivative of $\hat{\psi}_T^h$ is:

$$(\hat{\psi}_T^h)'(\xi) = \hat{\psi}_T^h(\xi)\left(\frac{\kappa\theta}{\sigma^2}\Big((A_-)'(\xi)T - 2\frac{B'(\xi)}{B(\xi)}\Big) + \frac{v(0)}{\sigma^2}\Big((A_-)'(\xi)C(\xi) + A_-(\xi)C'(\xi)\Big)\right). \tag{A.4}$$

We first need the first derivatives of d and g:

$$d'(\xi) = \frac{(\mathrm{i}\rho\sigma\xi - \kappa)\mathrm{i}\rho\sigma + \sigma^2(\mathrm{i}/2 + \xi)}{d(\xi)}, \quad (A_\pm)'(\xi) = -\mathrm{i}\rho\sigma \pm d'(\xi), \tag{A.5}$$

$$g'(\xi) = \frac{(A_-)'(\xi)A_+(\xi) - A_-(\xi)(A_+)'(\xi)}{A_+(\xi)^2}. \tag{A.6}$$

The first derivative of B is given by

$$B'(\xi) = \frac{(b_1)'(\xi)b_2(\xi) - b_1(\xi)(b_2)'(\xi)}{b_2(\xi)^2}, \tag{A.7}$$
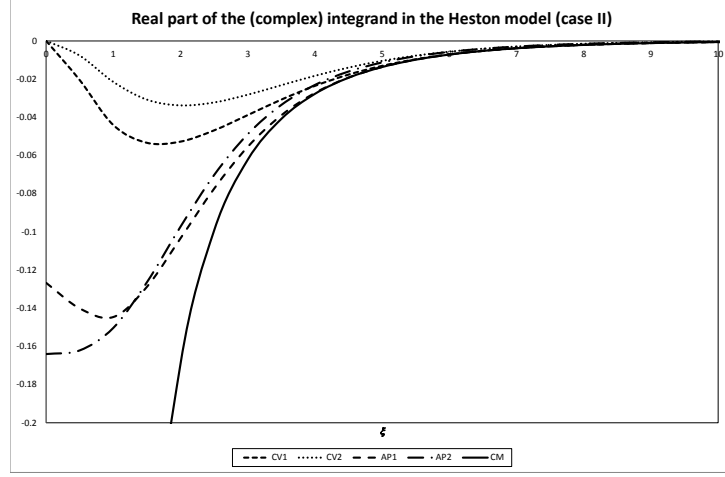
FIGURE 4. The solid line represents the real part of (2.5) with $\eta = 0.5$. The square dot line represents the real part of (3.8) with the Black-Scholes volatility given by (3.4). The dash line represents the real part of the same integrand with the Black-Scholes volatility equal to 0.3. The round dot line represents the real part of (3.10) with the Black-Scholes volatility given by (3.5). The dash dot line represents the real part of the same integrand with the Black-Scholes volatility equal to 0.3. The Heston stochastic volatility model parameters are case III in table 4.1.

where $(b_1)' = e^{-dT}(gd'T - g')$ and $(b_2)' = -g'$. The first derivative of C is given by

$$C'(\xi) = \frac{(c_1)'(\xi)b_1(\xi) - c_1(\xi)(b_1)'(\xi)}{b_1(\xi)^2}, \tag{A.8}$$

where $(c_1)' = d'Te^{-dT}$.

A.2. **The Variance-Gamma model.** The Variance-Gamma characteristic function (4.7) has much simpler functional form compared with the Heston characteristic function, and the first derivative is

$$(\hat{\psi}_T^{vg})'(\xi) = \hat{\psi}_T^{vg}(\xi)\left(i\omega T - \frac{T}{\nu}\frac{\sigma^2\nu\xi - i\theta\nu}{1 + \sigma^2\nu\xi^2/2 - i\theta\nu\xi}\right). \tag{A.9}$$

REFERENCES

[1] H. Albrecher, P. Mayer, W. Schoutens and J. Tistaert. (2006). The little Heston trap. Wilmott Magazine, January Issue, 83–92.
[2] L. Andersen. (2007). Simple and efficient simulation of the Heston stochastic volatility model. Journal of Computational Finance, **11**, 1–42.
[3] L. Andersen and J. Andreasen. (2002). Volatile volatilities. Risk, December, 163–168.
[4] L. Andersen and V. Piterbarg. (2010). *Interest Rate Modelling.* Vol I: Foundations and Vanilla Models. Atlantic Financial Press, Lodon and New York.
[5] F. Black and M. Scholes. (1973). The pricing of options and corporate liabilities. Journal of Political Economy, **81**, 637–654.
[6] K. Borovkov and A. Novikov. (2002). On a new approach to calculating expectations for option pricing. Journal of Applied Probability, **39** (4), 889–895.
[7] P. Carr and D. Madan. (1999). Option valuation using the fast Fourier transform. Journal of Computational Finance, **2** (4), 61–73.
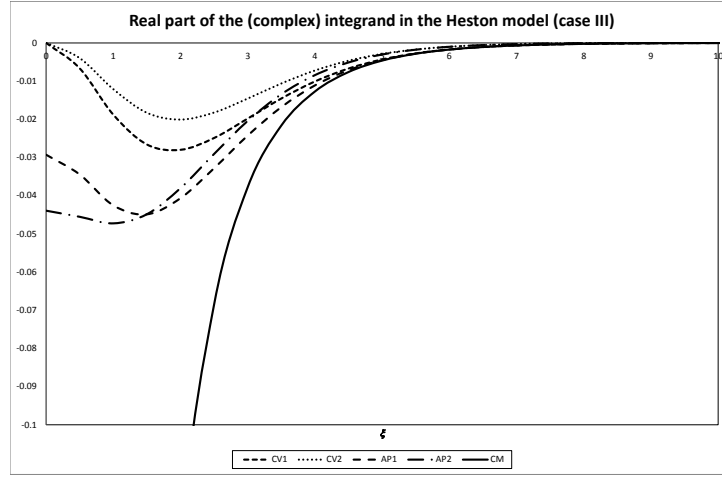
FIGURE 5. The solid line represents the real part of (2.5) with $\eta = 0.5$. The square dot line represents the real part of (3.8) with the Black-Scholes volatility given by (3.4). The dash line represents the real part of the same integrand with the Black-Scholes volatility equal to 0.25. The round dot line represents the real part of (3.10) with the Black-Scholes volatility given by (3.5). The dash dot line represents the real part of the same integrand with the Black-Scholes volatility equal to 0.25. The Variance-Gamma model parameters are case I in table 4.1.

[8] P. Carr, E. Chang and D. Madan. (1998). The variance gamma process and option pricing. European Finance Review, **2**, 79–105.

[9] D. Dufresne, J. Garrido and M. Morales. (2009). Fourier inverstion formulas in option pricing and insurance. Methodology and Computing in Applied Probability, **11** (3), 359–383.

[10] J. Gatheral. (2006). *The Volatility Surface: A Practitioner's Guide.* John Wiley and Sons, Inc., New Jersey.

[11] S. Heston. (1993). A closed-form solution for options with stochastic volatility and applications to bond and currency options. Review of Financial Studies, **6** (2), 327–343.

[12] A. Itkin. (2005). Pricing options with VG model using FFT. arXiv working paper: `arXiv:physics/0503137v2`.

[13] F. Kilin. (2011). Accelerating the calibration of stochastic volatility models. Journal of Derivatives, **18** (3), 7–16.

[14] R. Lee. (2004). Option pricing by transform methods: extension, unification and error control. Journal of Computational Finance, **7** (3), 51–86.

[15] A. Lewis. (2000). *Option Valuation under Stochastic Volatility: with Mathematica code.* Finance Press, London.

[16] A. Lewis. (2001). A simple option formula for general jump-diffusion and other exponential Lévy processes. OptionCity.net working paper: `www.optioncity.net/pubs/ExpLevy.pdf`.

[17] R. Lord and C. Kahl. (2010). Complex logarithms in Heston-like models. Mathematical Finance, **20** (4), 671–694.

[18] K. Matsuda. (2004). Introduction to option pricing with Fourier transform: option pricing with exponential Lévy models. Online working paper: `www.maxmatsuda.com/Papers/2004/Matsuda\%20Intro\%20FT\%20Pricing.pdf`.

[19] J. McCulloch. (2003). The risk-neutral measure and option pricing under log-stable uncertainty. Ohio State University working paper: `econ.ohio-state.edu/jhm/papers/rnm.pdf`.

[20] H. Priestley. (2003). *Introduction to Complex Analysis.* Second edition. Oxford University Press, Oxford.

[21] E. Stein and J. Stein. (1991). Stock price distribution with stochastic volatility: An analytic approach. Review of Financial Studies, **4**, 727–752.

CENTRE FOR ACTUARIAL STUDIES, DEPARTMENT OF ECONOMICS, UNIVERSITY OF MELBOURNE, VICTORIA 3010, AUSTRALIA

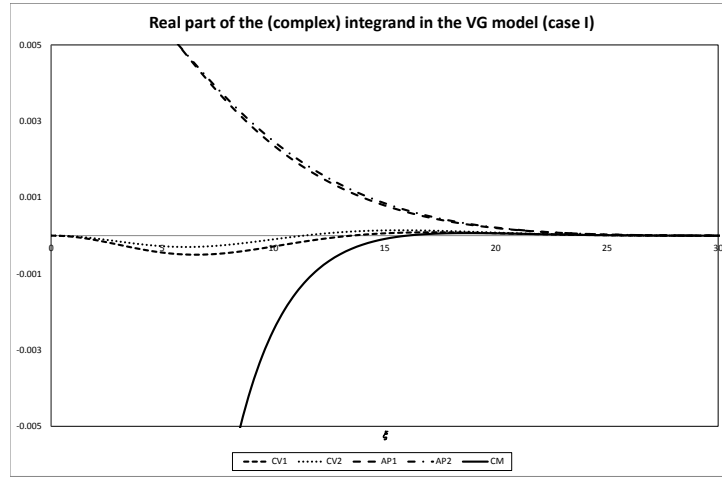*E-mail address*: `mark@markjoshi.com, chaoyangps@gmail.com`
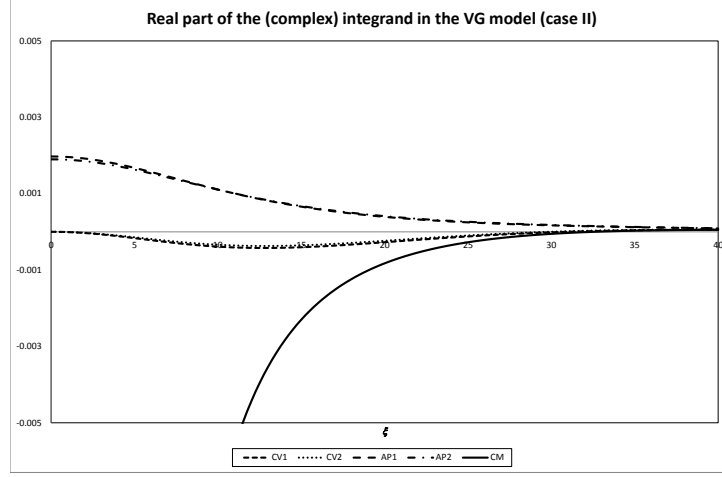
FIGURE 6. The solid line represents the real part of (2.5) with $\eta = 0.5$. The square dot line represents the real part of (3.8) with the Black-Scholes volatility given by (3.4). The dash line represents the real part of the same integrand with the Black-Scholes volatility equal to 0.12. The round dot line represents the real part of (3.10) with the Black-Scholes volatility given by (3.5). The dash dot line represents the real part of the same integrand with the Black-Scholes volatility equal to 0.12. The Variance-Gamma model parameters are case II in table 4.1.

Heston	number of integration points										
case I	5	6	7	8	9	10	11	12	13	14	15
strike	Ratio of AP1 error to CV2 error										
0.80	0.58	0.94	0.58	0.72	0.91	**1.12**	0.63	0.76	0.80	0.84	0.90
0.85	1.38	0.85	1.11	0.53	0.67	**1.14**	1.02	-0.16	0.81	1.89	0.61
0.90	0.96	0.90	0.98	1.15	0.02	**0.61**	0.45	0.99	0.91	1.22	1.14
0.95	0.91	0.80	0.60	1.16	1.17	**1.80**	0.30	0.69	0.89	0.51	0.54
1.00	0.89	0.57	0.68	0.64	1.15	**1.38**	1.24	1.33	0.06	1.05	1.37
1.05	0.85	1.17	1.11	0.39	0.55	**0.54**	0.36	2.71	0.94	0.72	0.39
1.10	0.74	1.01	1.17	1.39	2.16	**2.72**	0.20	0.63	0.90	1.24	2.10
1.15	2.71	0.99	1.28	1.31	1.35	**1.38**	1.36	1.27	1.07	0.60	0.97
1.20	1.15	0.93	0.75	0.64	0.51	**0.34**	0.23	0.32	1.12	1.09	1.06
strike	Ratio of AP2 error to CV2 error										
0.80	0.83	0.97	0.93	0.96	0.97	**0.96**	0.99	0.96	1.01	1.00	1.00
0.85	1.34	0.99	1.08	0.97	1.03	**0.95**	1.01	0.92	1.00	1.08	0.99
0.90	1.10	1.00	1.05	1.01	1.08	**1.02**	0.98	1.01	0.99	1.13	1.03
0.95	1.12	0.99	0.88	1.00	0.98	**0.98**	0.98	0.98	0.98	1.02	1.02
1.00	0.80	0.96	0.96	1.00	1.16	**1.00**	1.02	1.02	0.95	0.99	0.97
1.05	0.95	1.04	10.31	1.01	1.02	**1.00**	0.97	1.12	1.01	1.02	1.04
1.10	0.95	1.02	1.02	0.99	0.95	**1.00**	0.99	1.00	1.02	1.02	1.05
1.15	1.34	1.15	1.04	0.98	0.98	**1.00**	1.01	1.00	0.98	0.96	0.91
1.20	1.04	0.97	0.98	1.02	1.02	**0.99**	0.98	0.99	1.02	2.03	1.05

TABLE 4.3. The numbers represent the ratios of the AP1 or AP2 pricing errors to the CV2 pricing errors given in table 4.2. The average of the highlighted AP1 ratios is 1.23, and the average of the highlighted AP2 ratios is 0.99. The Heston stochastic volatility model parameters are case I in table 4.1.

Heston	case II	number of integration points										
strike	true price	5	6	7	8	9	10	11	12	13	14	15
strike	true price	5	6	7	8	9	10	11	12	13	14	15
0.80	955	-0.17	-0.92	-0.20	0.06	0.04	**0.02**	0.01	0.01	0.01	0.00	0.00
0.85	1098	0.47	-0.32	-0.18	-0.04	0.01	**0.03**	0.02	0.01	0.01	0.00	0.00
0.90	1262	-0.23	-0.07	0.01	0.00	0.00	**0.02**	0.02	0.01	0.01	0.00	0.00
0.95	1449	-1.31	-0.35	-0.01	0.03	0.03	**0.03**	0.02	0.01	0.01	0.00	0.00
1.00	1665	-1.64	-0.62	-0.15	-0.02	0.02	**0.03**	0.02	0.01	0.01	0.00	0.00
1.05	1413	-1.03	-0.47	-0.15	-0.03	0.01	**0.02**	0.02	0.01	0.01	0.00	0.00
1.10	1197	-0.28	-0.16	-0.03	0.01	0.03	**0.03**	0.02	0.01	0.01	0.00	0.00
1.15	1017	-0.18	-0.12	-0.01	0.02	0.03	**0.03**	0.02	0.01	0.01	0.00	0.00
1.20	870	-0.81	-0.38	-0.11	-0.02	0.02	**0.03**	0.02	0.01	0.01	0.00	0.00

TABLE 4.4. The pricing errors (in basis points) from the CV2 algorithm. The true prices are computed from approximating (3.9) with a 150-point Gauss-Laguerre quadrature rule. The Heston stochastic volatility model parameters are case II in table 4.1.

Heston	number of integration points										
case II	5	6	7	8	9	10	11	12	13	14	15
strike	Ratio of AP1 error to CV2 error										
0.80	8.36	0.29	1.87	6.74	6.97	**10.72**	6.83	4.35	3.51	2.27	2.07
0.85	4.53	2.03	2.30	12.89	22.10	**6.49**	4.91	5.15	5.22	3.47	3.53
0.90	7.23	10.00	44.12	198.69	81.21	**11.08**	6.00	5.02	4.49	2.85	2.13
0.95	0.65	1.09	42.16	-14.99	11.58	**8.01**	6.63	6.37	6.01	4.32	5.52
1.00	0.47	0.22	3.70	34.57	17.08	**7.79**	6.26	6.25	6.32	5.42	219.46
1.05	1.44	0.65	1.11	17.65	36.97	**10.14**	7.26	6.71	6.26	4.56	8.83
1.10	8.05	3.81	15.13	-59.02	14.14	**7.93**	6.44	6.08	5.44	3.34	3.51
1.15	12.19	5.63	41.47	-32.83	12.92	**7.76**	6.40	6.14	5.65	3.58	5.59
1.20	1.89	1.23	5.09	34.98	25.43	**9.84**	7.17	6.57	5.96	1.09	1.06
strike	Ratio of AP2 error to CV2 error										
0.80	13.54	0.53	2.26	0.77	3.33	**1.71**	2.74	2.81	1.68	0.11	0.95
0.85	1.65	2.86	1.57	4.11	8.68	**0.09**	2.14	2.49	1.50	0.08	1.20
0.90	3.82	14.01	45.95	53.24	25.59	**0.26**	2.06	1.91	1.00	0.09	0.80
0.95	1.14	1.71	22.03	2.92	2.00	**0.85**	2.00	1.80	0.89	0.19	1.94
1.00	0.91	0.37	0.11	8.60	2.14	**1.10**	1.81	1.56	0.84	0.07	57.46
1.05	0.61	0.60	0.52	4.49	3.87	**1.30**	1.75	1.37	0.72	0.12	1.07
1.10	1.17	3.19	0.24	10.58	0.43	**1.31**	1.55	1.17	0.65	0.29	0.09
1.15	3.12	4.33	2.05	4.95	0.06	**1.39**	1.51	1.16	0.75	0.58	0.86
1.20	0.09	0.63	1.34	6.57	0.29	**1.55**	1.54	1.15	0.82	0.83	1.73

TABLE 4.5. The numbers represent the ratios of the AP1 or AP2 pricing errors to the CV2 pricing errors given in table 4.4. The average of the highlighted AP1 ratios is 8.86, and the average of the highlighted AP2 ratios is 1.06. The Heston stochastic volatility model parameters are case II in table 4.1.

Heston	case III	number of integration points										
strike	true price	5	6	7	8	9	10	11	12	13	14	15
0.80	1229	1.09	0.05	-0.11	0.03	0.05	**0.01**	-0.01	0.00	0.00	0.00	0.00
0.85	1435	0.82	-0.01	-0.06	0.04	0.04	**0.00**	-0.01	0.00	0.00	0.00	0.00
0.90	1662	0.60	-0.04	-0.03	0.05	0.03	**0.00**	0.00	0.00	0.00	0.00	0.00
0.95	1910	0.43	-0.05	0.00	0.05	0.02	**0.00**	-0.01	0.00	0.00	0.00	0.00
1.00	2180	0.30	-0.06	0.02	0.05	0.02	**0.00**	-0.01	0.00	0.00	0.00	0.00
1.05	1970	0.21	-0.06	0.04	0.05	0.02	**0.00**	0.00	0.00	0.00	0.00	0.00
1.10	1781	0.16	-0.05	0.05	0.05	0.01	**0.00**	0.00	0.00	0.00	0.00	0.00
1.15	1610	0.14	-0.05	0.06	0.05	0.01	**0.00**	0.00	0.00	0.00	0.00	0.00
1.20	1458	0.13	-0.05	0.06	0.05	0.01	**0.00**	0.00	0.00	0.00	0.00	0.00

TABLE 4.6. The pricing errors (in basis points) from the CV2 algorithm. The true prices are computed from approximating (3.9) with a 150-point Gauss-Laguerre quadrature rule. The Heston stochastic volatility model parameters are case III in table 4.1.

Heston	number of integration points										
case III	5	6	7	8	9	10	11	12	13	14	15
strike	Ratio of AP1 error to CV2 error										
0.80	0.51	0.38	1.26	0.40	0.88	**3.44**	1.40	0.74	1.80	5.12	1.51
0.85	0.53	8.50	2.07	0.08	1.16	**5.77**	2.02	1.68	8.99	5.23	1.37
0.90	0.55	3.90	4.70	0.28	1.53	**15.79**	2.16	1.74	2.44	1.08	2.70
0.95	0.59	3.75	398.86	0.41	2.08	**30.19**	2.06	1.36	0.79	0.26	1.24
1.00	0.66	3.98	6.10	0.49	2.78	**12.82**	2.28	1.37	0.59	0.36	1.18
1.05	0.82	4.28	1.11	0.52	3.50	**13.29**	3.04	1.87	0.87	0.28	1.39
1.10	1.08	4.48	2.98	0.51	4.06	**19.98**	4.80	3.37	2.10	0.28	3.09
1.15	1.41	4.39	2.80	0.44	4.49	**32.67**	7.67	6.82	7.16	54.46	0.76
1.20	1.66	3.83	2.92	0.33	5.10	**23.76**	7.18	5.58	4.73	1.09	1.06
strike	Ratio of AP2 error to CV2 error										
0.80	0.97	15.82	0.65	3.44	0.29	**4.32**	1.18	1.25	4.30	3.39	3.30
0.85	1.26	45.00	1.28	1.59	0.60	**5.86**	0.79	1.89	11.11	0.57	3.04
0.90	1.62	9.16	2.95	0.83	0.88	**12.18**	0.06	2.17	3.90	2.02	0.01
0.95	2.09	4.88	229.02	0.37	1.19	**16.38**	0.47	1.84	1.82	1.00	0.74
1.00	2.75	3.14	2.98	0.03	1.50	**4.64**	0.79	1.69	1.40	0.88	0.79
1.05	3.64	2.16	1.44	0.22	1.75	**3.23**	1.05	1.77	1.34	0.89	0.86
1.10	4.65	1.54	0.93	0.40	1.89	**3.53**	1.37	2.15	1.55	0.97	1.21
1.15	5.38	1.13	0.69	0.52	1.97	**4.66**	1.67	2.79	1.96	4.03	0.89
1.20	5.44	0.88	0.61	0.60	2.12	**2.89**	1.28	1.67	0.41	1.75	9.99

TABLE 4.7. The numbers represent the ratios of the AP1 or AP2 pricing errors to the CV2 pricing errors given in table 4.6. The average of the highlighted AP1 ratios is 17.52, and the average of the highlighted AP2 ratios is 6.41. The Heston stochastic volatility model parameters are case III in table 4.1.

VG	case I	number of integration points										
strike	true price	5	6	7	8	9	10	11	12	13	14	15
0.80	112	1.00	-1.46	0.12	0.26	-0.11	**-0.02**	0.04	-0.01	0.00	0.01	0.00
0.85	190	2.68	-0.25	-0.45	0.10	0.07	**-0.04**	-0.01	0.01	0.00	0.00	0.00
0.90	306	1.48	0.75	-0.17	-0.14	0.03	**0.03**	-0.01	-0.01	0.00	0.00	0.00
0.95	468	-0.65	0.58	0.22	-0.06	-0.05	**0.00**	0.01	0.00	0.00	0.00	0.00
1.00	683	-1.69	-0.17	0.18	0.08	-0.01	**-0.02**	0.00	0.00	0.00	0.00	0.00
1.05	455	-1.05	-0.54	-0.09	0.04	0.03	**0.00**	0.00	0.00	0.00	0.00	0.00
1.10	283	0.37	-0.24	-0.17	-0.05	0.00	**0.01**	0.01	0.00	0.00	0.00	0.00
1.15	162	1.26	0.27	-0.01	-0.04	-0.02	**-0.01**	0.00	0.00	0.00	0.00	0.00
1.20	85	0.95	0.44	0.14	0.03	0.00	**-0.01**	0.00	0.00	0.00	0.00	0.00

TABLE 4.8. The pricing errors (in basis points) from the CV2 algorithm. The true prices are computed from approximating (3.9) with a 150-point Gauss-Laguerre quadrature rule. The Variance-Gamma model parameters are case I in table 4.1.

VG	number of integration points										
case I	5	6	7	8	9	10	11	12	13	14	15
strike	Ratio of AP1 error to CV2 error										
0.80	0.15	1.20	0.31	0.90	0.70	**1.14**	0.79	0.62	0.86	0.82	0.41
0.85	1.49	0.62	0.98	0.58	0.90	**0.70**	0.93	0.82	0.07	0.66	1.61
0.90	1.83	1.33	0.50	0.90	0.60	**0.84**	0.76	1.04	0.48	0.42	3.45
0.95	2.07	0.78	1.00	0.59	0.85	**0.49**	0.90	5.37	0.55	0.54	2.53
1.00	1.98	2.84	0.64	0.91	0.15	**0.82**	1.08	0.87	0.99	1.21	1.18
1.05	1.41	0.91	1.11	0.76	0.90	**1.30**	0.58	0.62	0.32	5.92	7.36
1.10	5.38	0.73	0.69	1.03	3.42	**0.73**	0.75	0.40	4.28	2.12	0.48
1.15	2.90	1.83	3.32	0.95	0.87	**0.98**	1.65	0.76	0.89	0.18	0.86
1.20	2.01	0.05	0.36	1.26	6.51	**0.64**	0.66	0.53	0.17	1.09	1.06
strike	Ratio of AP2 error to CV2 error										
0.80	1.03	1.46	1.36	1.08	1.02	**1.00**	1.01	0.97	0.93	1.06	0.79
0.85	1.57	1.79	1.16	1.00	1.03	**0.99**	0.93	1.06	0.55	0.81	2.29
0.90	2.36	1.44	0.94	1.04	0.97	**0.97**	1.11	1.18	0.71	0.49	4.18
0.95	1.26	1.15	1.10	0.96	0.99	**1.17**	1.07	2.99	0.72	0.68	2.84
1.00	2.07	2.50	0.88	1.00	0.97	**0.99**	0.95	1.02	1.03	1.09	1.10
1.05	1.99	1.14	0.94	1.05	1.03	**1.18**	0.80	0.72	0.47	6.59	7.60
1.10	3.83	0.21	0.81	1.03	0.42	**0.90**	0.82	0.32	5.21	2.31	0.47
1.15	2.83	1.96	3.75	1.15	0.99	**0.99**	0.97	1.03	1.06	0.02	0.91
1.20	2.59	0.46	0.44	1.07	3.88	**0.85**	0.77	0.57	0.16	0.46	0.78

TABLE 4.9. The numbers represent the ratios of the AP1 or AP2 pricing errors to the CV2 pricing errors given in table 4.8. The average of the highlighted AP1 ratios is 0.85, and the average of the highlighted AP2 ratios is 1.00. The Variance-Gamma model parameters are case I in table 4.1.

VG	case II	number of integration points										
strike	true price	5	6	7	8	9	10	11	12	13	14	15
0.80	16	13.74	7.75	-1.16	-5.19	-3.11	**0.67**	2.06	0.90	-0.62	-0.89	-0.18
0.85	37	4.56	9.50	7.99	3.14	-1.05	**-2.52**	-1.67	-0.13	0.80	0.78	0.23
0.90	81	-14.04	-4.75	1.61	4.27	3.98	**2.25**	0.43	-0.69	-0.99	-0.71	-0.23
0.95	168	-19.56	-14.80	-9.70	-5.17	-1.78	**0.32**	1.27	1.43	1.12	0.66	0.22
1.00	328	2.38	-1.04	-3.11	-3.95	-3.89	**-3.33**	-2.55	-1.77	-1.09	-0.55	-0.17
1.05	101	28.74	20.16	13.59	8.94	5.81	**3.72**	2.34	1.43	0.81	0.41	0.15
1.10	13	13.93	6.49	2.31	0.39	-0.35	**-0.57**	-0.61	-0.59	-0.54	-0.49	-0.44
1.15	1.25	-13.24	-14.49	-12.08	-8.62	-5.60	**-3.42**	-1.97	-1.02	-0.41	-0.03	0.19
1.20	0.12	-18.74	-12.66	-5.35	-0.29	2.04	**2.60**	2.33	1.77	1.17	0.65	0.24

TABLE 4.10. The pricing errors (in basis points) from the CV2 algorithm. The true prices are computed from approximating (3.9) with a 150-point Gauss-Laguerre quadrature rule. The Variance-Gamma model parameters are case II in table 4.1.

VG	number of integration points										
case II	5	6	7	8	9	10	11	12	13	14	15
strike	Ratio of AP1 error to CV2 error										
0.80	0.65	0.13	5.48	1.10	0.57	**2.30**	1.04	0.87	0.97	0.91	0.99
0.85	3.64	1.28	0.72	0.07	2.61	**1.20**	0.99	0.65	0.96	0.94	1.00
0.90	0.10	1.35	4.96	1.65	1.20	**1.03**	0.83	1.02	0.97	0.97	1.03
0.95	1.29	1.07	0.92	0.79	0.54	**2.42**	1.15	1.04	1.01	1.01	1.08
1.00	8.04	13.35	3.31	1.95	1.47	**1.24**	1.13	1.08	1.06	1.07	1.17
1.05	0.72	0.86	1.11	1.08	1.13	**1.16**	1.16	1.15	1.14	1.16	1.29
1.10	1.94	2.65	4.04	10.60	3.47	**0.29**	1.07	1.25	1.23	1.17	1.12
1.15	0.35	0.37	0.80	1.09	1.27	**1.32**	1.25	1.11	0.91	1.06	1.27
1.20	0.57	1.15	1.98	14.73	0.24	**1.02**	1.21	1.20	1.12	1.09	1.06
strike	Ratio of AP2 error to CV2 error										
0.80	0.69	0.21	6.34	1.22	0.58	**2.84**	1.19	0.92	1.20	1.05	0.99
0.85	3.96	1.37	0.74	-0.03	3.06	**1.34**	1.06	0.09	1.12	1.05	1.03
0.90	0.18	1.57	5.48	1.78	1.27	**1.04**	0.61	1.22	1.09	1.05	1.04
0.95	1.29	1.07	0.90	0.74	0.39	**3.21**	1.30	1.13	1.07	1.05	1.05
1.00	8.53	14.24	3.53	2.07	1.55	**1.31**	1.18	1.11	1.07	1.05	1.07
1.05	0.67	0.81	0.94	1.03	1.09	**1.12**	1.12	1.10	1.09	1.07	1.07
1.10	1.88	2.63	4.13	11.52	4.47	**0.19**	0.75	1.03	1.07	1.05	1.03
1.15	0.38	0.31	0.72	1.02	1.21	**1.29**	1.26	1.17	1.06	0.55	1.06
1.20	0.49	1.04	1.85	14.59	0.10	**0.89**	1.11	1.14	1.09	1.02	0.96

TABLE 4.11. The numbers represent the ratios of the AP1 or AP2 pricing errors to the CV2 pricing errors given in table 4.10. The average of the highlighted AP1 ratios is 1.33, and the average of the highlighted AP2 ratios is 1.47. The Variance-Gamma model parameters are case II in table 4.1.

Model	Integration along $\mathbb{R}$	Matching $(\hat{\psi}_T)'(-\mathfrak{i})$
Heston case I	Yes	?
Heston case II	Yes	Yes
Heston case III	Yes	Yes
VG case I	?	?
VG case II	Yes	Yes

TABLE 4.12. Summary of the numerical tests. The first column presents the results of whether performing the integration along the real axis results an improved accuracy level ('Yes') or not ('?'). The second column presents the results of whether computing the Black-Scholes volatility via matching the first derivatives of the two characteristic functions results an improved accuracy level ('Yes') or not ('?').